Theor Chem Acc (2002) 108:179–186
DOI 10.1007/s00214-002-0371-9

Theoretical Chemistry Accounts

Regular article

Direct ab initio dynamics calculations on the rate constants for the hydrogen-abstraction reaction of C_2H_5F with O (^3P)

Jing-yao Liu[1], **Ze-sheng Li**[1], **Zhen-wen Dai**[2], **Xu-ri Huang**[1], **Chia-chung Sun**[1]

[1]Institute of Theoretical Chemistry, State Key Laboratory of Theoretical and Computational Chemistry, Jilin University, Changchun 130023, China
[2]Department of Physics, Jilin University, Changchun 130023, China

Received: 23 January 2002 / Accepted: 23 June 2002 / Published online: 20 September 2002

Abstract. The hydrogen-abstraction reaction $C_2H_5F + O \rightarrow C_2H_4F + OH$ has been studied by a dual-level direct dynamics method. For the reaction, three reaction channels, one for α-abstraction and two for β-abstraction, have been identified. The potential-energy surface information is obtained at the MP2(full)/6-311G(d,p) and PMP2(full)/6-311G(3df,3pd) (single-point) levels. By canonical variational transition-state theory, rate constants for each reaction channel are calculated with a small-curvature tunneling correction. The total rate constant is calculated from the sum of the individual rate constants and the temperature dependence of the branching ratios is obtained over a wide range of temperatures from 300 to 5,000 K. The agreement of the rate constants with experiment is good in the experimental temperature range from 1,000 to 1,250 K. The calculated results indicate that at low temperatures α-abstraction is most likely to be the major reaction channel, while β-abstraction channels will significantly contribute to the whole reaction rate as the temperature increases.

Key words: Hydrogen abstraction – Direct dynamics – Ab initio – Rate constant – Variational transition state

1 Introduction

Chlorofluorocarbons (CFCs) are being phased out because of their well-known connection to the depletion of stratospheric ozone and the contribution to the greenhouse effect that are detrimental to the environment [1]. Hydrofluorocarbons (HFCs) have been proposed as major CFC replacements used in refrigeration, air conditioning, foam blowing, and cleaning applications since they retain many of desirable physical and chemical properties of CFCs and have a zero ozone depletion potential [2]. Owing to their containing at least one C–H bond, HFCs are readily attacked by oxidizing agents in the lower atmosphere or in combustion systems, and thus they have shorter atmospheric lifetimes. The reaction with the OH radical, which is the main channel of tropospheric degradation for HFCs, has attracted considerable attention, experimentally [3, 4] and theoretically [5, 6, 7, 8]. On the other hand, less attention has been paid to the reactions of HFCs with O atoms, which play an important role in the field of fire suppressants and air pollution [9] relevant to flame and combustion chemistry, except for the reactions of oxygen and fluoromethanes [10, 11, 12]. In the most recent work [13], the direct measurement of the overall rates of O (^3P) with fluoroethane (C_2H_5F) and difluoroethanes (CH_2FCH_2F and CH_3CHF_2) was reported in the temperature range from 1,000 to 1,400 K. In the present work, the focus is on the hydrogen-abstraction reaction of oxygen with fluoroethane.

In fluoroethane, the hydrogen atom can be abstracted from α- and β-carbon atoms; thus for the reaction $C_2H_5F + O$, two hydrogen-abstraction reactions, R1 and R2, i.e., α- and β-abstractions,

$$CH_3CH_2F + O \rightarrow CH_3CHF + OH \quad R1 \ , \tag{1}$$

$$CH_2FCH_3 + O \rightarrow CH_2FCH_2 + OH \quad R2 \ , \tag{2}$$

are feasible. However, because it is difficult to know which hydrogen atom is abstracted in experiments, only α-abstraction was assumed [13]. Up to now no information is available on the branching ratio R1/R2; therefore, theoretical investigations are very desirable to gain an understanding of the multiple channel reaction mechanisms of the hydrogen-abstraction reaction of $C_2H_5F + O$. Furthermore, since there are no available experimental data at temperatures other than in the range from 1,000 to 1,250 K, our theoretical results are expected to provide a good prediction for the kinetics of this reaction over a wide temperature range.

Here, a dual-level (X//Y) direct dynamics method [14] is applied to study the α- and β-hydrogen-abstraction reactions, R1 and R2. As usual, X//Y refers to optimization

Correspondence to: Z. Li
e-mail: ljy121@mail.jlu.edu.cn

and frequencies at lower-level Y with single-point energies calculated at higher-level X. In this approach, the required electronic structure information for the stationary points and some extra points along the minimum energy path (MEP) is obtained directly from ab initio calculations. Subsequently, by means of the Polyrate 8.4.1 program [15], the rate constants for each reaction channel were calculated using the variational transition-state theory (VTST) [16, 17] with the interpolated single-point-energies (ISPE) [18] method. The canonical VTST (CVT) [19] and the small-curvature tunneling (SCT) method [20, 21] were taken into account at the VTST level. Finally, the total rate constant of the reaction $C_2H_5F + O$ was obtained as well as the temperature dependence of the branching ratios of reactions R1 and R2.

2 Calculation methods

In the present study, all the electronic structure calculations were carried out with the program package Gaussian 98 [22]. The geometries of all the stationary points (the reactants, transition states (TSs), and products) involved in reactions R1 and R2 were optimized at the restricted or unrestricted second-order Møller–Plesset perturbation level, including all the electrons in a correlation calculation, with the standard 6-311G(d,p) basis set [(U)MP2(full)/6-311G(d,p)]. The harmonic vibrational frequencies were calculated at the same level of theory to characterize the nature of each critical point and to make zero-point-energy corrections. The number of imaginary frequencies (0 or 1) indicates whether a minimum or a TS has been located. In order to yield more reliable reaction enthalpies and barrier heights, single-point calculations for the stationary points were made at the PMP2(full)/6-311G(3df,3pd) and QCISD(T)/6-311G(2df,2p) levels. For each reaction channel, the MEP was calculated with a gradient step size of 0.05 $amu^{1/2}$bohr at the MP2(full)/6-311G(d,p) level to confirm that the TSs really connect with minima along the reaction paths. At the same level, the energy derivatives, including gradients and Hessians at geometries along the MEP, were obtained to calculate the curvature of the reaction path and to calculate the generalized vibrational frequencies along the reaction path. Then, the energies along the MEP were refined with the ISPE method [18] at the PMP2(full)/6-311G(3df, 3pd) level.

This initial information on the potential-energy surface (PES) was used to evaluate the rate constants by means of the Polyrate 8.4.1 program [15]. The theoretical rate constants for each reaction path were calculated using the CVT with the SCT approximation proposed by Garrett and coworkers [19, 20, 21]. The generalized normal mode analysis was carried out in curvilinear coordinates [23] so as to eliminate unphysical imaginary values over a wide range of the reaction coordinate owing to the rectilinear coordinates. The lowest bending frequencies were real over the whole of the reaction path using the curvilinear coordinates. All vibrational modes other than the lowest vibrational one were treated harmonically, and for the lowest-frequency modes the partition functions were calculated using the hindered-rotor approximation of Truhlar and Chuang [24]. The spin–orbit splitting of $O(^3P)$, which is 158.26 and 226.98 cm^{-1} for $^3P_1$ and $^3P_0$ relative to $^3P_2$, was included when calculating the electronic partition functions. Finally, the total rate constant was obtained from the sum of the individual rate constants associated with the α- and β-abstraction reactions.

3 Results and discussion

3.1 Stationary points

The optimized geometries at the MP2(full)/6-311G(d, p) level of the reactants and products involved in reactions R1 and R2 are presented in Fig. 1 along with the available experimental data [25, 26]. The corresponding harmonic vibrational frequencies are given in Table 1. As shown in Fig. 1, fluoroethane (C_2H_5F) has C_s symmetry, and the fluoroethane radical (CH_2FCH_2) has two conformations with C_1 and C_s symmetry, respectively. When a comparison is possible, the geometries of C_2H_5F and OH are in good agreement with the corresponding experimental values; the maximum error of the bond lengths is 0.6%. With respect to the frequencies, the MP2(full) level gives an overestimate, with the largest deviation being about 10% between the calculated and experimental values.

Since the two hydrogen atoms in the α-position of C_2H_5F are equivalent, only one TS (α-TS1) of reaction R1 was located. As to the three β-hydrogen atoms, H′ (in Fig. 1) is different from the other two; as a result, two TSs β-TS2 and β-TS3 for reaction R2 were found. Thus, β-abstraction reactions via β-TS2 and β-TS3 are described as reactions R2a and R2b, corresponding to the product radical CH_2FCH_2 with C_s and C_1 symmetry, respectively. The reaction path symmetry numbers for the reactions are 2 for R1, 1 for R2a, and 2 for R2b. The optimized structures of the three TSs at the MP2(full)/6-311G(d,p) level are depicted in Fig. 2, and the corresponding harmonic vibrational frequencies are listed in Table 2. In the three TS structures, the reactive C–H′ bond, which is broken, is elongated by 13.97%, 16.91%, and 16.68% compared to the C–H equilibrium bond length of C_2H_5F, and the forming bond O–H′ is 27.7%, 22.93%, and 23.25% longer than the equilibrium bond length of the OH radical. Thus, all the TSs are reactant-like, and the three reactions will proceed via "early" TSs. Furthermore, it is obvious that the α-TS1 is a more reactant-like TS, so the α-hydrogen abstraction reaction R1 will proceed via an "earlier" TS compared with β-hydrogen-abstraction reactions R2a and R2b. The TSs are identified with only one imaginary frequency, and the imaginary frequencies of the three TSs are 2,233*i*, 2,146*i*, and 2,176*i* cm^{-1}, respectively.

It is well known that the estimates for the reaction enthalpies, ΔH^0_{298}, and barrier heights, ΔE, are sensitive to the level of theory and basis set used. Here, the reaction enthalpies and potential barriers were calculated at three levels, i.e., (U)MP2(full)/6-311G(d,p), (U)MP2/6-311G(3df,3pd)//MP2, and QCISD(T)/6-311G(2df,2p)//MP2. The corresponding results and the experimental data are listed in Table 3. It is shown that the MP2(full)/6-311G(d,p) calculations predict the α-hydrogen-abstraction reaction (R1) to be endothermic, and the QCISD(T) calculations estimate this reaction to be nearly thermally neutral, while the results of the unprojected MP2 energies and spin-projected MP2 energies (PMP2) calculated at the MP2(full) level with a larger basis set, 6-311G(3df,3pd), find reaction R1 to be exothermic, and the improved reaction enthalpies are −3.21 and −4.52 kcal mol^{-1}, respectively. Furthermore, the PMP2 result is in excellent agreement with the experimental value of -4.23 ± 2.0 kcal mol^{-1} derived from the experimental standard heats of formation (CH_3CH_2F, -63.06 ± 2.0 kcal mol^{-1} [27]; CH_3CHF, -17.01 ± 2.0 kcal mol^{-1} [27]; OH, 9.33 kcal mol^{-1} [26];

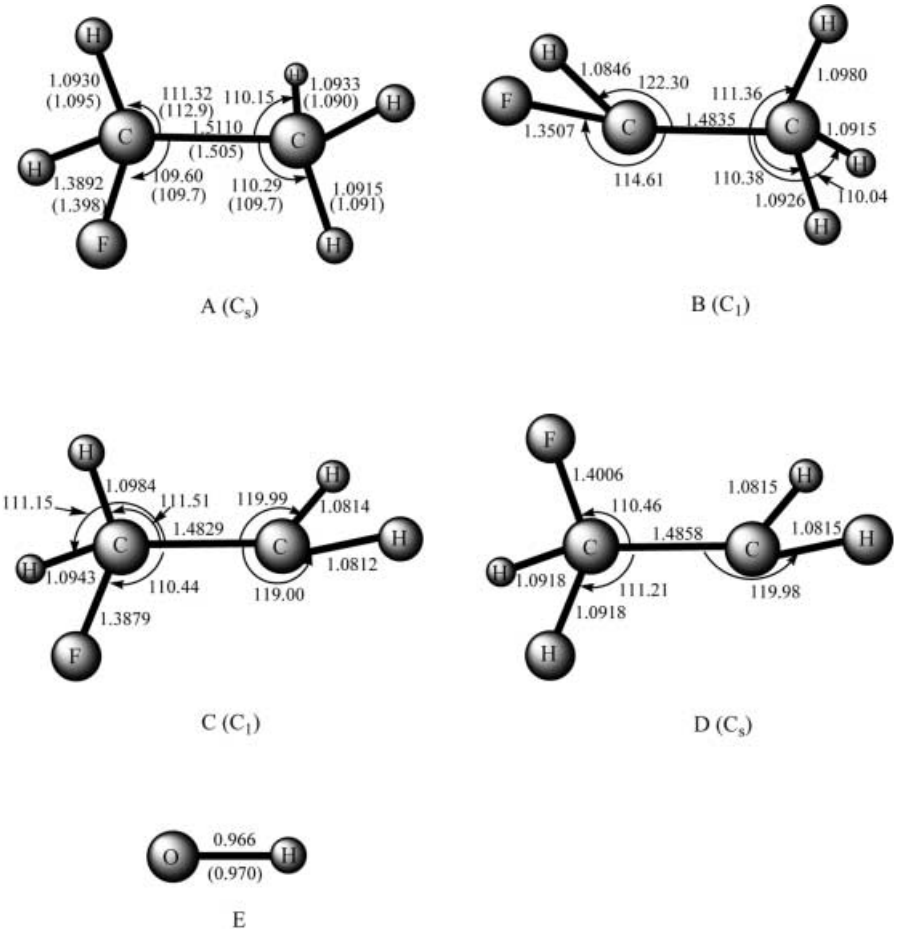

Fig. 1. Optimized geometries of CH_3CH_2F (*A*), CH_3CHF (*B*), CH_2FCH_2 with C_1 symmetry (*C*) and C_s symmetry (*D*), and OH (*E*) at the MP2(full)/6-311G(d,p) level. The values in the *parentheses* are the experimental values (Ref. [25] for CH_3CH_2F and Ref. [26] for OH). Bond lengths are in angstroms and angles are in degrees

Table 1. Calculated frequencies (cm^{-1}) of the reactants and products at the MP2(full)/6-311G(d,p) level. The values in *parentheses* are experimental values (Ref. [25] for CH_3CH_2F and Ref. [26] for OH)

Species	Frequency (cm^{-1})					
$CH_3CH_2F(C_s)$	279	418	827	914	1,112	1,154
	(243)	(415)	(810)	(880)	(1,048)	(1,048)
	1,217	1,334	1,420	1,467	1,501	1,522
	(1,108)	(1,277)	(1,365)	(1,395)	(1,449)	(1,449)
	1,552	3,095	3,106	3,161	3,188	3,200
	(1,479)	(2,915)	(2,941)	(3,003)	(3,003)	(3,003)
CH_3CHF	209	418	644	932	1,054	1,157
	1,217	1,392	1,450	1,487	1,518	3,058
	3,147	3,193	3,239			
CH_2FCH_2 (C_1)	181	417	494	862	1,000	1,134
	1,152	1,283	1,436	1,488	1,525	3,055
	3,128	3,222	3,344			
CH_2FCH_2 (C_s)	88	385	645	813	1,026	1,116
	1,210	1,323	1,434	1,511	1,538	3,116
	3,179	3,218	3,336			
OH	3,857					
	(3,735)					

O, 59.61 kcal mol^{-1} [26]). Similarly, at the PMP2/6-311G(3df,3pd) level, the calculated reaction enthalpy values of 0.24 kcal mol^{-1} for R2a and −0.63 kcal mol^{-1} for R2b are in reasonable agreement with the estimated value, 1.37 ± 2.0 kcal mol^{-1} (CH_2CH_2F, −11.41 ± 0.24 kcal mol^{-1} [28]). The barrier heights of the three reaction channels are brought down by about 4.0 kcal mol^{-1} at the MP2 level when the size of the basis set is increased from 6-311G(d,p) to the 6-311G(3df,3pd). The spin-projection correction at the MP2 (full)/6-311G(3df,3pd) level reduces the barrier heights further by about 2.5 kcal mol^{-1}. The difference between the MP2 and PMP2 results for the barrier heights is larger than that for the reaction enthalpies (about 1.5 kcal mol^{-1}). This is because of more severe spin contamination in the TS regions compared to the product radicals. For example, the $\langle S^2 \rangle$ values before spin annihilation for three TSs are around 2.05, whereas the values of $\langle S^2 \rangle$ for the product radicals never exceed 0.762. Also, Table 3 shows that the calculated results for the reaction enthalpies and barrier heights obtained at the more computationally demanding QCISD(T)/6-311G(2df,2p) level are obviously higher than the corresponding PMP2(full)/6-311G(3df,3pd) results, and the best agreement between theory and experiment is obtained at the PMP2(full)/6-311G(3df,3pd) level. Thus, for the reaction system under study, we chose the PMP2(full) method with the 6-311G(3df,3pd) basis set to refine the energies along the MEP in the following kinetic calculation.

Furthermore, from Table 3 one can see that the α-abstraction reaction is more exothermic and has a lower barrier height compared to β-abstraction. The barrier height of 6.66 kcal mol^{-1} obtained at the PMP2(full)/6-311G(3df,3pd) level for α-abstraction is

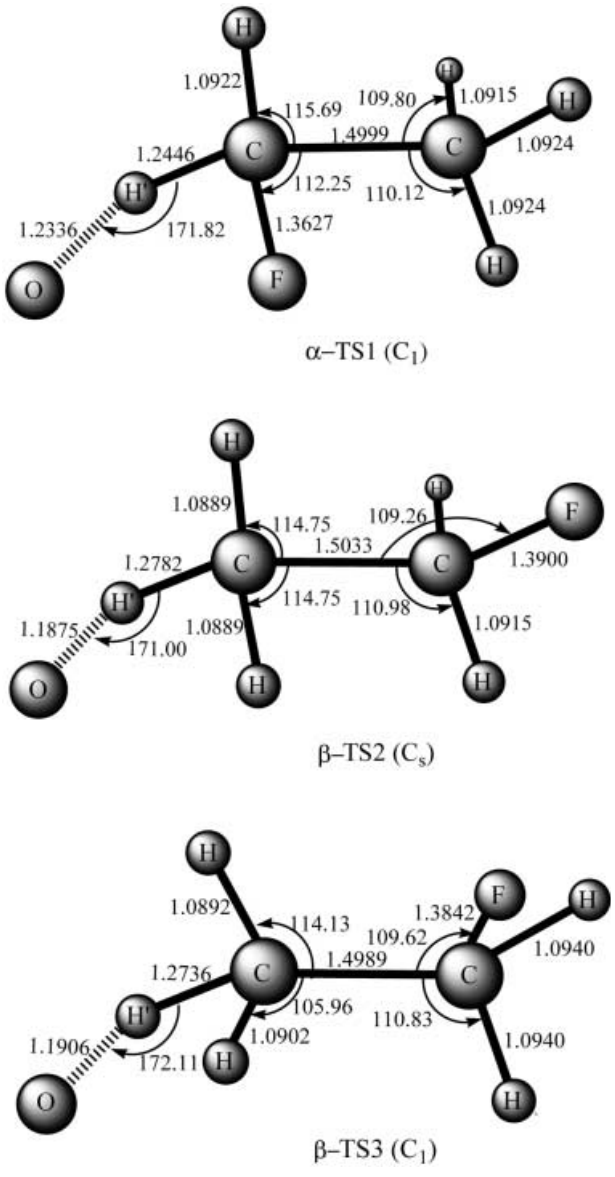

Fig. 2. Optimized geometries of the three transition states at the MP2(full)/6-311G(d,p) level. Bond lengths are in angstroms and angles are in degrees

Table 2. Calculated frequencies (cm^{-1}) of the transition states at the MP2(full)/6-311G(d,p) level

Species	Frequency (cm^{-1})
α-TS1	2,233*i*, 112, 175, 267, 417, 573, 849, 930, 1,132, 1,186, 1,188, 1,220, 1,337, 1,401, 1,444, 1,492, 1,513, 3,094, 3,153, 3,187, 3,201
β-TS2	2,146*i*, 90, 105, 369, 438, 650, 825, 884, 1,100, 1,113, 1,209, 1,232, 1,238, 1,334, 1,445, 1,506, 1,540, 3,132, 3,154, 3,185, 3,250
β-TS3	2,176*i*, 83, 143, 399, 482, 614, 830, 916, 1,084, 1,134, 1,164, 1,246, 1,269, 1,322, 1,443, 1,474, 1,531, 3,097, 3,146, 3,157, 3,243

more than 2.0 kcal mol^{-1} lower than those of the two channels for β-abstraction. This is in accordance with the fact that in CH_3CH_2F the dissociation energy (Dv_{298}) of the αC–H bond is lower than that of a βC–H bond by about 5 kcal mol^{-1}. The corresponding values of (Dv_{298}) obtained at the PMP2(full)/6-311G(3df,3pd)//MP2 level are 96.88 and 101.63 kcal mol^{-1}, which agree reasonably well with the experimental ones [28], 96.87 ± 1.5 and 103.7 ± 0.5 kcal mol^{-1}, respectively. The difference between α- and β-bond dissociation energies can be analyzed by the changes in the electron density distribution due to fluorine substitution. Because of the high electronegativity of the fluorine atom, the electron density on the α-carbon atom is significantly reduced and that on the α-hydrogen atom is increased. The electron density redistribution leads to the lowering of the polarization of the αC–H bond and makes it easier to break. Similarly, the net electron redistribution caused by the F atom results in stronger C–H bonds on the β-carbon than on the α-carbon. Therefore, the barrier heights are higher for β-abstraction than for α-abstraction, and as a result, hydrogen abstraction from the α-position will be preferred at lower temperatures. This view is further testified in the following study of the rate constants.

3.2 Properties of the reaction path

The MEP for each reaction channel was obtained at the MP2(full)/6-311G(d,p) level and the potential profile was further corrected with the ISPE method [18] at the PMP2(full)/6-311G(3df,3pd) level. The classical potential-energy curves, $V_{MEP}(s)$, and the vibrationally adiabatic ground-state potential-energy curves, $V_a^G(s)$, of reactions R1, R2a, and R2b are shown in Fig. 3 as a function of the intrinsic reaction coordinate (IRC), s, at the PMP2(full)/6-311G(3df,3pd)//MP2 level.

The changes in the bond length along the MEP of the α-hydrogen abstraction reaction R1 as functions of s are described in Fig. 4. It appears that for the reaction the active C–H′ and H′–O bonds change strongly in the course of the hydrogen-abstraction reaction, and the other bond lengths of C–C, C–F, and C–H are almost invariable during the reaction process. The length of the breaking C–H′ bond elongates linearly with s after about $s = -1.0$ $amu^{1/2}$ bohr, and the forming bond H′–O shortens rapidly and arrives at the O–H equivalent bond length of the OH radical at about $s = 1.0$ $amu^{1/2}$ bohr. It is thus evident that the geometric changes mainly take place in the region of $s = -1.0$ to 1.0 $amu^{1/2}$ bohr on the IRC. The same conclusion can be drawn from reactions R2a and R2b.

The variations of the generalized normal-mode vibrational frequencies along the MEP of reaction R1 are shown in Fig. 5. In the negative limit of s ($s = -\infty$), the frequencies are associated with those of CH_3CH_2F, and in the positive limit of s ($s = +\infty$), the frequencies correspond to the products $OH + CH_3CHF$. Most of these frequencies do not change significantly on going from the reactants to the products. The two lowest harmonic frequencies are the transitional modes, which correspond to free rotations and translations that evolve into vibrations. Of all the frequencies, the frequency of mode 1, shown as the solid line in Fig. 5, has a dramatic drop in the region from $s = -1.0$ to 1.0 $amu^{1/2}$ bohr as

Table 3. Reaction enthalpies, ΔH^0_{298}, and barrier heights, ΔE, (kcal mol^{-1}) for reactions R1 and R2 at various levels. The values in *parentheses* are the corresponding PMP2 results. The experimental heats of formation were obtained from Ref. [26] for OH and O, Ref. [27] for CH_3CH_2F and CH_3CHF, and Ref. [28] for CH_2FCH_2

		MP2(full)/ 6-311G(d,p)	MP2(full)/ 6-311G(3df,3pd)	QCISD(T)/ 6-311G(2df,2p)	Experimental
R1 (α-TS1)	ΔH^0_{298}	2.53 (1.27)	−3.21 (−4.52)	0.42	−4.23 ± 2.0
	ΔE	13.52 (10.76)	9.03 (6.66)	8.87	
R2a (β-TS2)	ΔH^0_{298}	7.40 (6.02)	1.71 (0.24)	5.30	1.37 ± 2.0
	ΔE	16.37 (13.36)	11.55 (8.84)	12.37	
R2b (β-TS3)	ΔH^0_{298}	6.78 (5.37)	0.88 (−0.63)	4.65	
	ΔE	15.97 (13.00)	11.75 (9.11)	12.65	

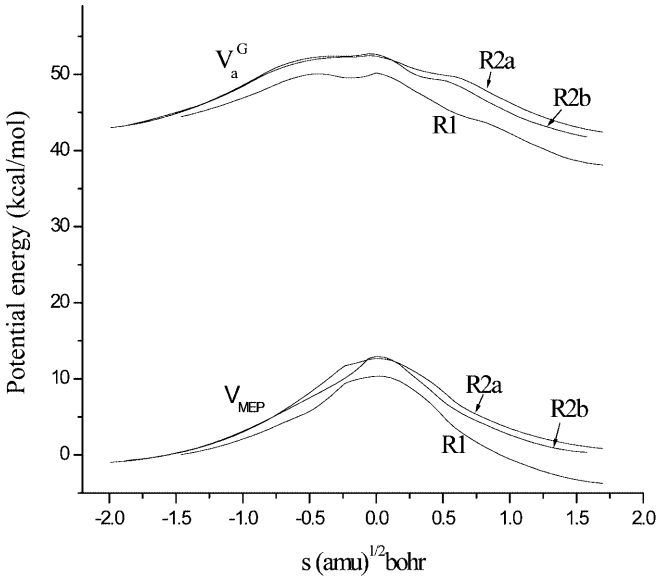

Fig. 3. Classical potential energy, V_{MEP}, and vibrationally adiabatic energy ground-state, V_a^G, as functions of s for reactions R1, R2a, and R2b at the PMP2(full)/6-311G(3df,3pd)//MP2(full)/6-311G(d,p) level

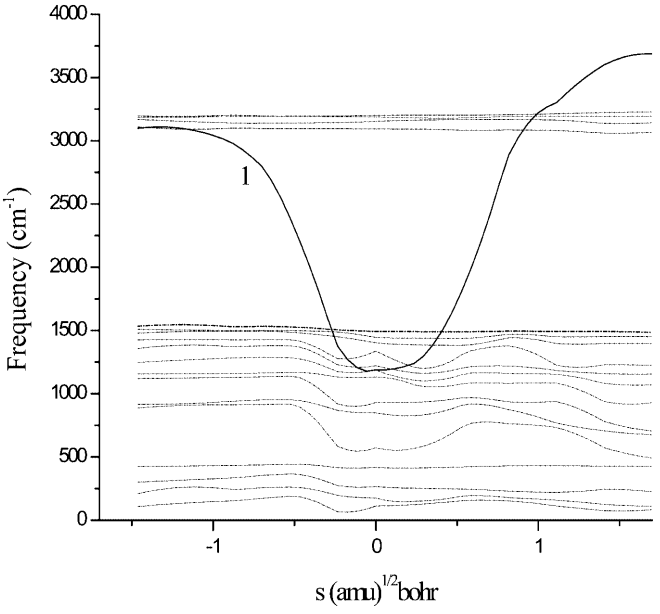

Fig. 5. Changes in the generalized normal-mode vibrational frequencies for reaction R1 as functions of s at the MP2(full)/6-311G(d,p) level

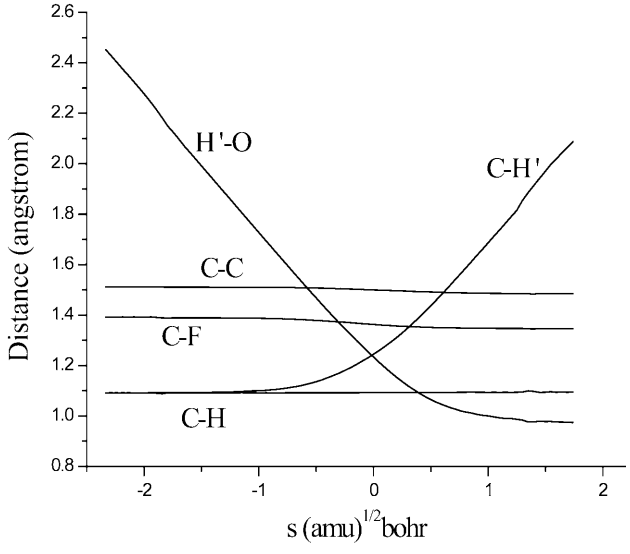

Fig. 4. Changes in the bond lengths (angstroms) for reaction R1 as functions of s at the MP2(full)/6-11G(d,p) level

the reaction proceeds. Mode 1 correlates with the evolution from the C–H′ stretching vibrational frequency of CH_3CH_2F to the stretching vibrational frequency of OH. Therefore, mode 1 can be referred to as the "reactive mode" in the reaction. Similar behavior is also observed for the two β-hydrogen-abstraction reactions.

In addition, for brevity, we only state without details that the reaction-path curvatures of the three reactions are not severe. The maximum values of the total curvature for reactions R1, R2a, and R2b are about 2.2, 2.7, and 2.0 au, respectively. Thus, the SCT correction method should be suitable for calculating the reaction rate constants.

3.3 Calculation of rate constants

Dual-level dynamics calculations were carried out for the reaction of $C_2H_5F + O$ using the VTST-ISPE approach. The total rate constant was obtained from the sum of the individual rate constants associated with the three channels via three TSs, α-TS1, β-TS2, and β-TS3, respectively. The PES information for each reaction

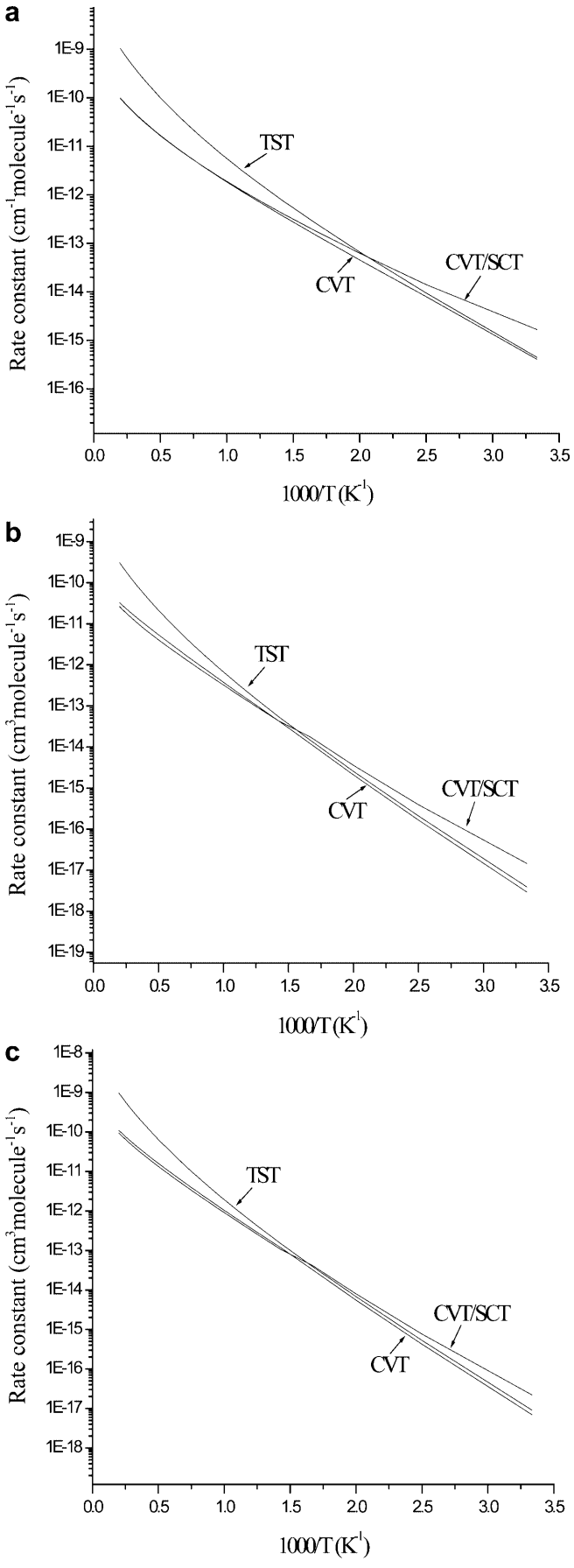

◀

Fig. 6. Plot of the transition-state theory (TST), canonical variational TST (*CVT*), and CVT/small-curvature tunneling (*SCT*) rate constants calculated at the PMP2(full)/6-311G(3df,3pd)// MP2(full) /6-311G(d,p) level versus $1{,}000/T$ between 300 and 5,000 K for reaction R1 via α-TS1. **b** Same as in **a** except for the reaction R2a via β-TS2. **c** Same as in **a** except for the reaction R2b via β-TS3

channel obtained at the PMP2(full)/6-311G(3df,3pd)// MP2(full)/6-311G(d,p) level was put into POLYRATE 8.4.1 program [15] to produce the VTST [16,17] rate constants over a wide temperature range from 300 to 5,000 K. The forward rate constants were calculated by the conventional TS theory (TST), the CVT, and the CVT/SCT.

The TST, CVT, and CVT/SCT rate constants of reaction R1 are shown in Fig. 6a, and the corresponding values of reactions R2a (via β-TS2) and R2b (via β-TS3) are plotted in Fig. 6b and c, respectively. From Fig. 6a–c, it can be seen that the difference between the TST and CVT rate constants increases as the temperature increases, while the CVT/SCT rate constants are slightly larger than the CVT rate constants in the range 300–600 K and they are asymptotic to the CVT ones at higher temperatures. This means that for the title reaction the variational effect is small at lower temperatures and becomes significant in the higher-temperature range, whereas the SCT effect is small and should be considered only in the lower temperature range.

The CVT/SCT rate constants of k_1, k_{2a}, and k_{2b} as well as the total rate constant, k, and the available experimental values [13] are given in Table 4. The theoretical and the experimental rate constants are plotted against $1{,}000/T$ in Fig. 7a, and the temperature dependence of the k_1/k and k_2/k branching ratios is exhibited in Fig. 7b. Table 4 shows that, in the lower-temperature range ($T < 600$ K), k_1 is about 1 order of magnitude larger than k_{2a} and k_{2b}, and the total rate constant is nearly equal to the rate constant of reaction R1. Thus, the α-hydrogen abstraction is likely to dominate the reaction at lower temperatures. However, as shown in Fig. 7b, the contribution of k_1 to the total rate constant decreases with the increase in the temperature, for example, the k_1/k ratio is 98% at 300 K, 61% at 1,000 K, 50% at 1,800 K, and 46% at 3,000 K. It is also shown that at temperatures higher than 1,800 K, the rate constants for reaction R2, $k_2 = k_{2a} + k_{2b}$, becomes faster than k_1. Consequently, all three reaction channels will contribute to the whole reaction rate as the temperature increases. The rate constants (k) of the reaction $C_2H_5F + O$ are in excellent agreement with the measured experimental values [13] in the range 1,000–1,250 K. The deviation factor between the calculated and experimental data is of 1.5–0.93. Therefore, it is reasonable to think that the theoretical results obtained at the PMP2 (full)/6-311G(3df,3pd)//MP2(full)/6-311G(d,p) level are reliable over the entire temperature region. Furthermore, the three-parameter fits for the CVT/SCT rate constants for the α- and β-abstractions as well as for the total reaction from 300 to 5,000 K give the expressions as

Table 4. Rate constants ($cm^3molecule^{-1}s^{-1}$) for the reaction $C_2H_5F + O$ in the temperature range 300–5,000 K. k_1, k_{2a}, and k_{2b} represent the canonical variational transition-state theory (*CVT*)/small-curvature tunneling (*SCT*) rate constants of reactions R1, R2a (via β-TS2), and R2b (via β-TS3), respectively, and k represents total rate constant calculated from the sum of the three CVT/SCT rate constants. The experimental values are estimated ones from Ref. [13]

T (K)	k_1	k_{2a}	k_{2b}	k	Experimental
300	1.68×10^{-15}	1.46×10^{-17}	2.22×10^{-17}	1.72×10^{-15}	
400	1.44×10^{-15}	3.96×10^{-16}	7.66×10^{-16}	1.56×10^{-14}	
500	6.34×10^{-14}	3.59×10^{-15}	7.95×10^{-15}	7.49×10^{-14}	
600	1.83×10^{-13}	1.76×10^{-14}	4.22×10^{-14}	2.43×10^{-13}	
800	7.51×10^{-13}	9.74×10^{-14}	2.57×10^{-13}	1.11×10^{-12}	
900	1.25×10^{-12}	1.89×10^{-13}	5.16×10^{-13}	1.96×10^{-12}	
1,000	1.91×10^{-12}	3.23×10^{-13}	9.09×10^{-13}	3.14×10^{-12}	2.05×10^{-12}
1,100	2.73×10^{-12}	5.03×10^{-13}	1.45×10^{-12}	4.68×10^{-12}	3.86×10^{-12}
1,200	3.71×10^{-12}	7.32×10^{-13}	2.16×10^{-12}	6.60×10^{-12}	6.54×10^{-12}
1,250	4.26×10^{-12}	8.64×10^{-13}	2.58×10^{-12}	7.70×10^{-12}	8.25×10^{-12}
1,400	6.14×10^{-12}	1.33×10^{-12}	4.08×10^{-12}	1.16×10^{-11}	
1,600	9.16×10^{-12}	2.10×10^{-12}	6.66×10^{-12}	1.79×10^{-11}	
1,800	1.27×10^{-11}	3.03×10^{-12}	9.82×10^{-12}	2.56×10^{-11}	
2,000	1.67×10^{-11}	4.09×10^{-12}	1.35×10^{-11}	3.43×10^{-11}	
2,500	2.81×10^{-11}	7.17×10^{-12}	2.45×10^{-11}	5.98×10^{-11}	
3,000	4.11×10^{-11}	1.07×10^{-11}	3.72×10^{-11}	8.90×10^{-11}	
3,500	5.48×10^{-11}	1.45×10^{-11}	5.11×10^{-11}	1.20×10^{-10}	
4,000	6.91×10^{-11}	1.84×10^{-11}	6.55×10^{-11}	1.53×10^{-10}	
4,500	8.31×10^{-11}	2.24×10^{-11}	8.03×10^{-11}	1.86×10^{-10}	
5,000	9.70×10^{-11}	2.65×10^{-11}	9.52×10^{-11}	2.19×10^{-10}	

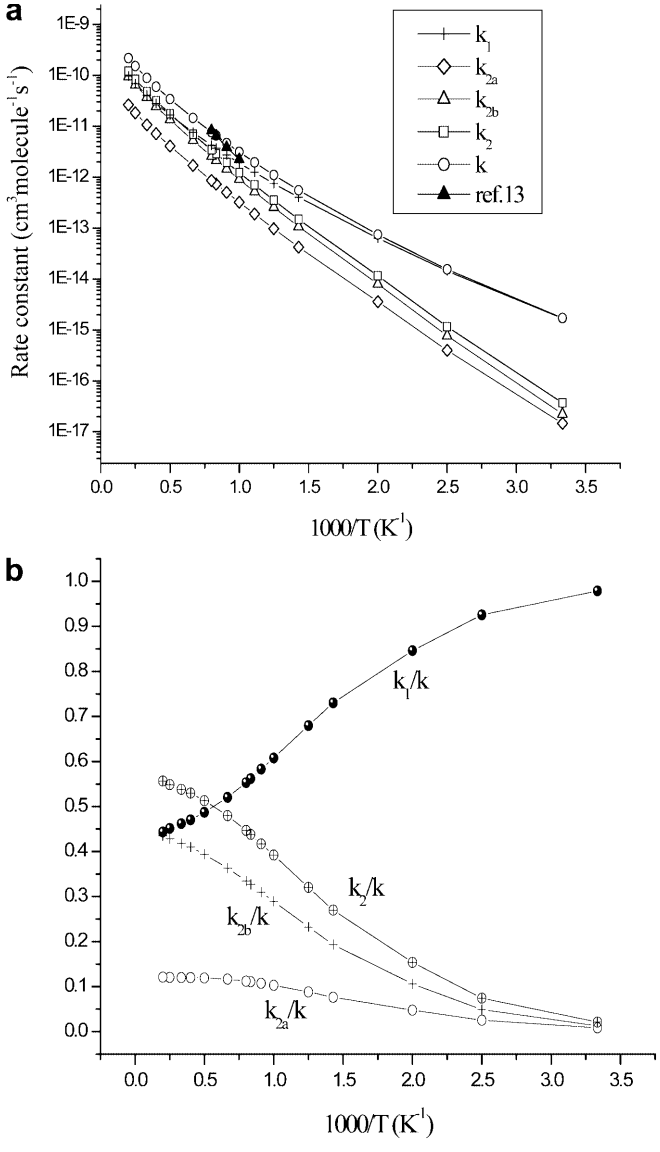

follows (in units of cubic centimeters per molecule per second):

$$k(\_) = 2.72 \times 10^{-15} T^{1.3} \exp(-2413.8/T),$$

$$k(\_) = 2.1 \times 10^{-13} T^{0.85} \exp(-4067.9/T),$$

$$k = 2.17 \times 10^{-15} T^{1.43} \exp(-2592.7/T) \ .$$

4 Conclusion

The dual-level direct ab initio dynamic method was employed to investigate α- and β-hydrogen-abstraction reactions of $C_2H_5F + O$. Three reaction channels proceeding via three early TSs (α-TS1, β-TS2, and β-TS3) have been identified. The PES information needed to calculate the rate constants was obtained at the MP2(full)/6-311g(d,p) level. Then, the energies along the MEP were improved using the ISPE method at the PMP2(full)/6-311G(3df,3pd) level. The changes in the potential energies and the generalized normal-mode vibrational frequencies along the MEP are very similar for the three reaction channels. The barrier height is lower by about 2.0 kcal mol^{-1} for α-abstraction than for β-abstraction owing to the difference in the C–H bond energy between the α- and β-positions. Accordingly, the α-abstraction reaction will be preferred in the lower-temperature range, while as the temperature increases, the contribution of the two β-abstraction reaction channels should be taken into account and the reaction will proceed in favor of β-abstraction at higher temperatures. Moreover, for the three reaction channels, the variational effect is important in the higher-temperature range, whereas the SCT effect is small. Since good

◄

Fig. 7. Plot of the calculated individual rate constants k_1, k_{2a}, and k_{2b}, the total rate constant k, and the available experimental values versus $1000/T$ between 300 and 5,000 K. **b** Calculated branching ratios versus $1000/T$ between 300 and 5000 K

agreement with the experimental data is obtained in the measured temperature range, 1,000–1,250 K, and there are no experimental data available in other temperature ranges, we hope our results may provide a good estimate for the kinetics of this reaction over a wide temperature range.

Acknowledgements. We thank Donald G. Truhlar for his provision of the POLYRATE 8.4.1 program. This work was supported by the National Natural Science Foundation of China (G29892168, 20073014), the Doctor Foundation by the Ministry of Education, the Foundation for University Key Teacher by the Ministry of Education, the Key Subject of Science and Technology by the Ministry of Education of China, and the Foundation for Young Teacher by Jilin University (2000A28).

References

1. (a) Tuck R, Plumb A, Condon E (1990) Geophys Rev Lett 17: 313; (b) Kerr JB (1991) Geophys Rev 96: 20703; (c) Stolarski R, Bojkoy R, Bishop L, Zerefos C, Staehelin J, Zawodny J (1991) Science 256: 342; (d) Kerr RA (1993) Science 262: 501; (e) Kerr JB, McElroy CT (1993) Science 262: 1032; (f) Newman A (1993) Environ Sci Technol 27: 1488; (g) Rosswall T (1991) Environ Sci Technol 25: 567; (h) Ravishankara AR, Turnipseed AA, Jensen NR, Barone S, Mills M, Howard CJ, Solomon S (1994) Science 263: 71
2. Manzer L (1990) Science 249: 31
3. Atkinson R, Baulch DL, Cox RA, Hampson RF Jr. Kerr JA, Rossi MJ, Troe JJ (1997) J Phys Chem Ref Data 26: 521
4. Atkinson RJ (1994) J Phys Chem Ref Data Monogr 2
5. Fu Y, Lewis-Bevan W, Tyrrell JJ (1995) Phys Chem 99: 630
6. Martell JM, Boyd RJ (1995) J Phys Chem 99: 13402
7. Sekušak S, Giisten H, Sabljicc A (1996) J Phys Chem 100: 6212
8. Chandra A, Uchimaru T, Sugie M (2000) J Comput Chem 21: 1305
9. Wilson WE, O'Donovan JT (1968) J Chem Phys 48: 2829
10. Miyoshi A, Ohmori K, Tsuchiya K, Matsui H (1993) Chem Phys Lett 204: 241
11. Medhurst LJ, Fleming J, Nelson HH (1997) Chem Phys Lett 266: 607
12. Kreye WC (1996) Chem Phys Lett 256: 383
13. Shiina H, Tsuchiya K, Oya M, Miyoshi A, Matsui H (2001) Chem Phys Lett 336: 242
14. (a) Truhlar DG (1995) In: Heidrich D (ed) The reaction path in chemistry: current approaches and perspectives. Kluwer, Dordrecht, pp 229–255; (b) Truhlar DG, Garrett BC, Klippenstein SJ (1996) J Phys Chem 100: 2771; (c) Hu WP, Truhlar DG (1996) J Am Chem Soc 118: 860
15. Chuang YY, Corchado JC, Fast PL, Villa J, Hu WP, Liu YP, Lynch GC, Jackels CF, Nguyen KA, Gu MZ, Rossi I, Coitino EL, Clayton S, Melissas VS, Lynch BJ, Steckler R, Garrett BC, Isaacson AD, Truhlar DG (2000) POLYRATE, version 8.4.1. University of Minnesota, Minneapolis
16. Truhlar DG, Garrett BC (1980) Acc Chem Res 13: 440
17. Truhlar DG, Isaacson AD, Garrett BC (1985) In: Baer M (ed) The theory of chemical reaction dynamics, vol 4. CRC, Boca Raton, p 65
18. Chuang YY, Corchado JC, Truhlar DG (1999) J Phys Chem 103: 1140
19. (a) Garrett BC, Truhlar DG (1979) J Chem Phys 70: 1593; (b) Garrett BC, Truhlar DG (1979) J Am Chem Soc 101: 4534; (c) Garrett BC, Truhlar DG, Grev RS, Magnuson AW (1980) J Phys Chem 84: 1730; (d) Erratum (1983) J Phys Chem 87: 4554
20. Lu DH, Truong TN, Melissas VS, Lynch GC, Liu YP, Garrett BC, Steckler R, Issacson AD, Rai SN, Hancock GC, Lauderdale JG, Joseph T, Truhlar DG (1992) Comput Phys Commun 71: 235
21. Liu YP, Lynch GC, Truong TN, Lu D, Truhlar DG, Garrett BC (1993) J Am Chem Soc 115: 2408
22. Frisch MJ, Truck GW, Schlegel HB, Scuseria GE, Robb MA, Cheeseman JR, Zakrzewski VG, Montgomery JA Jr, Stratmann RE, Burant JC, Dapprich S, Millam JM, Daniels AD, Kudin KN, Strain MC, Farkas O, Tomasi J, Barone V, Cossi M, Cammi R, Mennucci B, Pomelli C, Adamo C, Clifford S, Ochterski J, Petersson GA, Ayala PY, Cui Q, Morokuma K, Malick DK, Rabuck AD, Raghavachari K, Foresman JB, Cioslowski J, Ortiz JV, Boboul AG, Stefnov BB, Liu G, Liaschenko A, Piskorz P, Komaromi L, Gomperts R, Martin RL, Fox DJ, Keith T, Al-Laham MA, Peng CY, Nanayakkara A, Gonzalez C, Challacombe M, Gill PMW, Johson B, Chen W, Wong MW, Andres JL, Gonzalez C, Head-Gordon M, Replogle ES, Pople JA (1998) Gaussian 98. Gaussian, Pittsburgh, Pa
23. Chuang YY, Truhlar DG (1998) J Phys Chem A 102: 242
24. (a) Truhlar DG (1991) J Comput Chem 12: 266; (b) Chuang YY, Truhlar DG (2000) J Chem Phys 112: 1221
25. (a) Harmony MD, Kuczkowski RL, Schwedeman RH, Ramsay DA, Lovas FJ, Lafferty FWJ, Maki AG (1979) J Phys Chem Ref Data 8: 617; (b) Chase MW Jr, Davies CA, Downey JR Jr, Frarip DJ, McDonald RA, Syverud AN (1985) (eds) JANAF themochemical tables, vol 14, 3rd edn. National Bureau of Standards, Washington, DC; (c) Harmony MD (1990) J Chem Phys 93: 7522
26. Chase MW Jr (1998) J Phys Chem Ref Data Monogr 9
27. DeMorse WB, Sander SP, Golden DM, Molina MJ, Hampson RF, Kurylo M, Howard CJ, Ravishankara AR (1997) Chemical kinetics and photochemical data for use in stratospheric modeling, evaluation number 9. JPL publication 97-4
28. Zachariah MR, Westmoreland PR, Burgess DR Jr, Tsang W, Melius CF (1996) J Phys Chem 100: 8737